Received: 21 July 2023 | Revised: 10 December 2023 | Accepted: 3 February 2024

DOI: 10.1002/mop.34078

RESEARCH ARTICLE

WILEY

Optically transparent and angularly stable broad-stopband frequency selective surface for millimeter wave electromagnetic interference mitigation

Li Tang[1] | **Chengrong Wang**[1] | **Liping Yan**[1] | **Richard Xian-Ke Gao**[2] | **Xiang Zhao**[1] | **Changjun Liu**[1]

[1]College of Electronics and Information Engineering, Sichuan University, Chengdu, China

[2]Electronics and Photonics Department, Institute of High Performance Computing, Agency for Science, Technology and Research (A*STAR), Singapore, Singapore

Correspondence
Liping Yan, College of Electronics and Information Engineering, Sichuan University, Chengdu 610065, China.
Email: liping_yan@scu.edu.cn

Funding information
National Natural Science Foundation of China, Grant/Award Number: U22A2015

Abstract

An optically transparent and angularly stable frequency selective surface (FSS) with a broad stopband is introduced for addressing millimeter wave (mmW) electromagnetic interference. The unique FSS unit cell pattern incorporates a cross patch with Y-shaped branches, effectively broadening the bandwidth and enhancing the angular stability. Utilizing transparent conductive indium tin oxide deposited on both sides of a glass substrate enables the FSS to reflect and absorb electromagnetic waves. Consequently, the proposed FSS exhibits an exceptionally wide stopband ranging from 18.7 to 40.2 GHz, featuring an insertion loss of 14 dB and maintaining stable angular response up to 60° for both transverse electric and transverse magnetic polarizations. Moreover, an equivalent circuit model is developed to characterize the stopband behavior of the FSS. Finally, measurements conducted on a physical prototype of the proposed FSS validate its effectiveness, showing good agreement with the simulation results.

KEYWORDS

broad stopband, frequency selective surface (FSS), indium tin oxide (ITO), millimeter wave, transparency

1 | INTRODUCTION

Frequency selective surfaces (FSSs) are periodic structures consisting of planar metallic arrays on a dielectric substrate, designed to selectively transmit, reflect, and absorb electromagnetic waves at specific frequencies.[1] They find widespread applications in mitigating electromagnetic interference (EMI) across various communication bands, including GSM,[2] LTE-2.1 GHz,[3] WLAN/WiMax,[4,5] and sub-6 GHz in 5G new radio (NR),[6] often spanning multiple bands.[7] The ever advance of 5G NR communication has impelled the investigations into the millimeter wave (mmW) bands, such as n257 (26.5–29.5 GHz), n258 (24.25–27.5 GHz), and n260 (37–40 GHz).[8] Consequently, it is highly requisite to develop FSSs with broader stopbands for EMI mitigation in mmW band. While several opaque FSS designs have proven applicable for suppressing EMI in mmW band,[9–11] the challenge lies in directly applying these opaque designs for use in optically transparent scenarios.

Optically transparent FSSs have gained popularity in recent years, due to their compatibility with glass windows or other transparent surfaces in buildings or transportation vehicles, serving the purposes of EM shielding or information security. There are two major categories of transparent FSS design approaches: (1) one

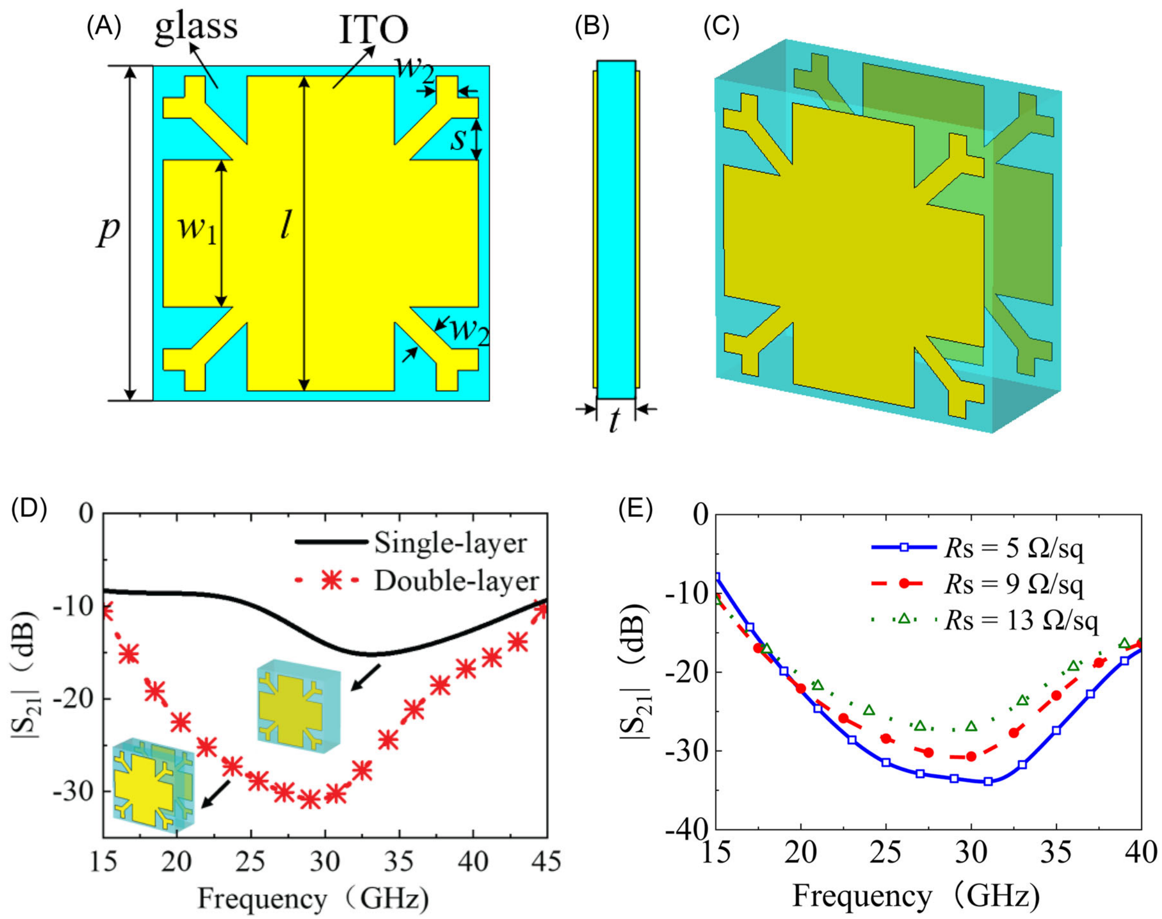

FIGURE 1 Geometry of the proposed frequency selective surface (FSS) unit cell: (A) top view, (B) side view, and (C) perspective view, where $p = 3.2$ mm, $l = 3$ mm, $w_1 = 1.2$ mm, $w_2 = 0.2$ mm, $s = 0.4$ mm, and $t = 1.4$ mm, respectively. (D) $|S_{21}|$ with respect to the number of layers of FSS with $R_S = 9\ \Omega$/sq. (E) $|S_{21}|$ with respect to the different R_S for double-layer FSS.

is to reduce the proportion of opaque metallic structures in an FSS unit cell deposited on a transparent substrate.[12–14] These approaches demonstrate effectiveness in the low-frequency band. However, their implementation poses challenges in mmW band due to limited space in an FSS unit cell and inevitable fabrication tolerances. Additionally, the use of opaque metal in FSS compromises the light transmittance and aesthetic appearance. To address these concerns, (2) another type of FSS designs employs electrotextiles or transparent conductive materials as alternatives, including silver nanowires (Ag NWs), gallium-doped zinc oxide (GZO), indium tin oxide (ITO), and so on.[15–22] While most of these transparent FSS structures primarily focus on offering stopbands in L, S, C, and X bands, few designs are available for effectively suppressing EMI at the specific mmW bands of 24.25–40 GHz used in 5G NR. Moreover, the limited existing transparent bandstop FSSs operating at mmW band exhibit narrow stopband and insufficient performance in terms of both shielding effectiveness and transparency.[14,15,18,19]

In this letter, a novel broad stopband FSS for EMI suppression in 5G mmW band is proposed, utilizing an optically transparent conductive ITO material. The ITO material is a commercially available substance with well-established manufacturing technologies. Noteworthy for its excellent electrical conductivity, high transmittance of visible light, and robust chemical and thermal stability,[23] ITO emerges as a promising alternative to opaque conductive metals in the design of transparent FSS. The suitability for use in challenging environments such as high temperatures and rainy seasons, underscores its potential of practicability and versatility.

The novelty of the proposed FSS design lies in two main aspects. Firstly, it introduces an optically transparent FSS featuring a wide stopband for the first attempt to mitigate EMI in the millimeter wave band. Secondly, the design capitalizes the conductivity characteristic of the ITO material to effectively reflect and absorb the incident electromagnetic waves. This results in a significant improvement in insertion loss (IL) within the desired frequency range. The performance of the proposed FSS is notable, achieving a wide stopband spanning from 18.7 to 40.2 GHz with an IL exceeding 14 dB, and exhibiting angular stability up to 60 degrees. Additionally, the FSS demonstrates an appealing optical transparency of 79.5% and displays insensitivity to polarization.

2 | DESIGN AND ANALYSIS OF TEH TRANSPARENT FSS

Considering the required functionality and performance, an FSS unit cell typically has a small dimensional size in mmW band. Therefore, complex FSS structures are not suggested due to both space limitation and processing tolerance. In light of this, a novel and concise FSS structure is proposed. The structure is composed of a cross patch with Y-shaped branches etched at the four corners, deposited on both the top and bottom of a glass substrate, as shown in Figure 1A–C. While a conductive patch with all four corners etched off can provide a stopband in the mmW band, it exhibits poor angular stability. To address it, an approach of fractal structure is introduced in our design owing to its efficacy in enhancing the angular stability.[24] Hence, a one-order fractal cross is overlapped on the patch, forming the Y-shaped branches etched at the corners. This innovative addition serves to not only improve the angular stability but also broaden the bandwidth.

The proposed FSS pattern is developed by using a conductive ITO coated on a nonconductive glass substrate with dielectric constant of $\varepsilon_r = 5.8$. Furthermore, a double-layer FSS structure design is incorporated, resulting in an additional improvement in IL and stopband width, as illustrated in Figure 1D. Meanwhile, the impact of ITO's sheet resistance (R_S) on the IL and bandwidth of the FSS has been analyzed, which is depicted in Figure 1E. The IL and the bandwidth are considerably improved as R_S decreases, while the resonant frequency slightly shifts higher. Taking feasibility and cost into account, the study chooses an ITO with $R_S = 9\ \Omega$/sq. The unit cell has a dimensional size of $0.17\,\lambda_L \times 0.17\,\lambda_L \times 0.076\,\lambda_L$, where λ_L corresponds to the free-space wavelength at the lower cut-off frequency of 16.3 GHz.

It can be observed from Figure 2A that this FSS structure is polarization insensitive due to its

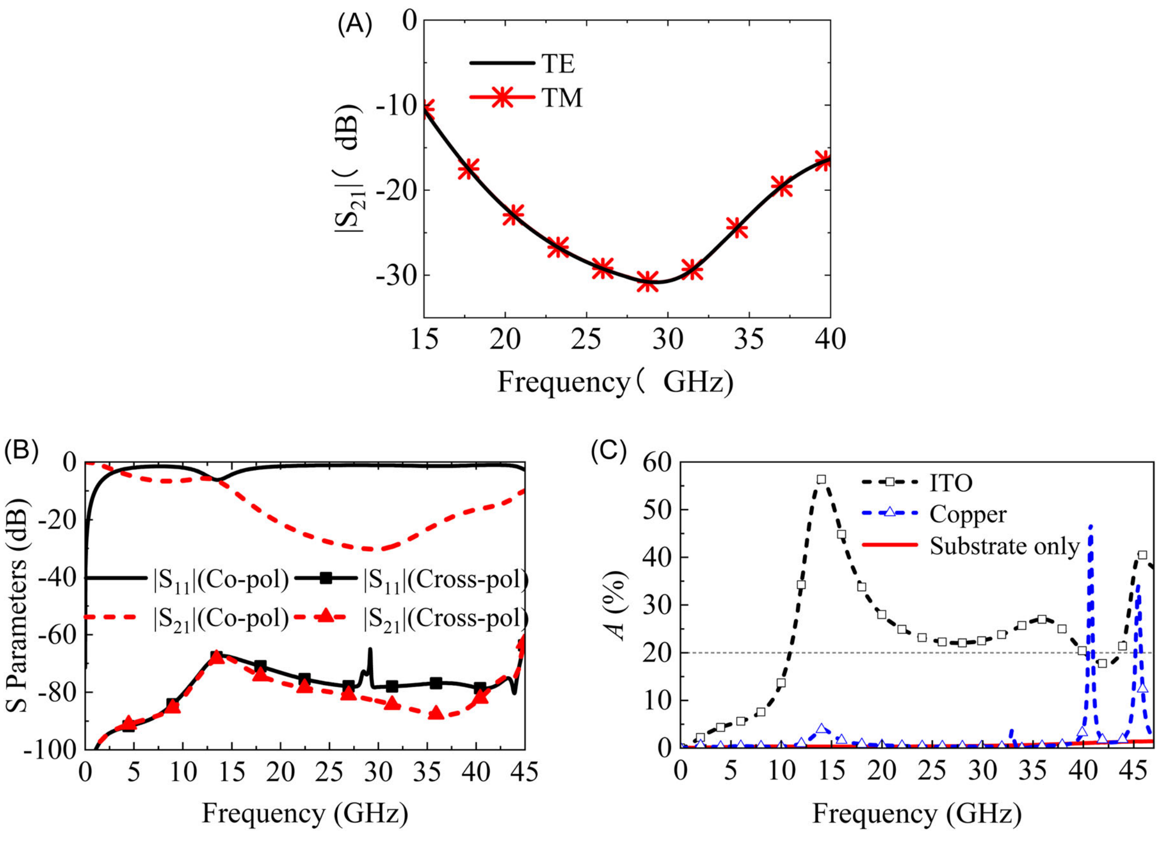

FIGURE 2 (A) $|S_{21}|$ for different polarizations at normal incidence. (B) S-parameters for co- and cross-polarizations, and (C) comparison of absorptivity for three cases at normal incidence: the frequency selective surface (FSS) with indium tin oxide (ITO), the FSS with copper, and glass substrate only.

90°-rotational symmetry. As shown in Figure 2B, the reflection and transmission coefficients fall below −60 dB simultaneously when copolarization changes to cross-polarization, which confirms that the IL of the proposed FSS is independent of the polarization transition. Moreover, the substitution of metal with ITO conductive film leads to additional energy loss, which is quantified using absorptivity.[25]

$$A(\omega) = 1 - R(\omega) - T(\omega), \tag{1}$$

where $R(\omega) = |r_{yy}(\omega)|^2 + |r_{xy}(\omega)|^2$ and $T(\omega) = |t_{yy}(\omega)|^2 + |t_{xy}(\omega)|^2$ are the reflected and transmitted power, respectively. r_{yy} and r_{xy} represent co- and cross-polarization of S_{11}, and t_{yy} and t_{xy} represent co- and cross-polarization of S_{21}. Figure 2C demonstrates that the absorptivity of the proposed FSS using ITO is notably higher than 20% in the stopband at normal incidence, unlike the use of copper where the absorption occurs only at individual frequency points. Comparing to the glass substrate only and the glass substrate with copper,

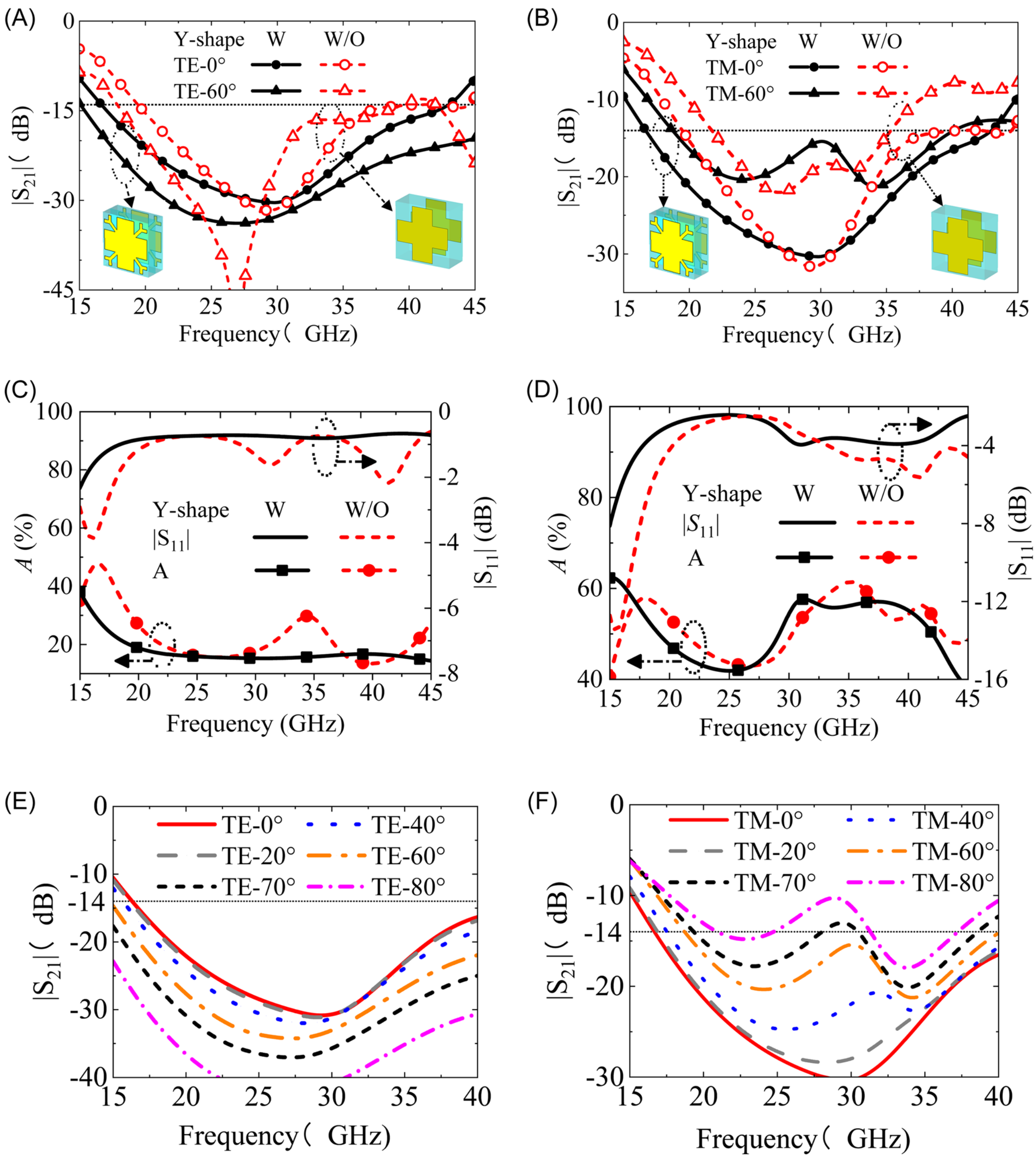

FIGURE 3 $|S_{21}|$ of the proposed frequency selective surfaces (FSSs) with (w) and without (w/o) Y-shaped branches etched at corners for (A) TE and (B) TM polarizations. $|S_{11}|$ and absorptivity of the FSSs with and without Y-shaped branches etched at corners for (C) TE and (D) TM polarizations at oblique incidence of 60°. $|S_{21}|$ with respect to incident angle for (E) TE and (F) TM polarizations.

it can be found that the use of ITO leads to a discernible increase in absorption. This absorption contributes, in part, to the IL of the proposed FSS.

To gain a deeper insight into the functionality of each element in the proposed FSS structure, Figure 3A,B present a comparison of the $|S_{21}|$ between the FSSs with and without the Y-shaped branches under different polarizations and incident angles. Obviously, the angular stability and bandwidth of the FSS with Y-shaped branches are significantly improved for both polarizations. Figure 3C,D depict reflection coefficient and absorptivity of the two FSS structures at 60° oblique incidence. For transverse electric (TE) polarization, the $|S_{11}|$ and absorptivity of the FSS structure with Y-shaped branches are quite stable in the frequency range of 18.0–45.0 GHz, while significant fluctuations are observed for the structure without Y-shaped branches. In contrast, for transverse magnetic (TM) polarization, the $|S_{11}|$ and absorptivity of both structures exhibit little fluctuations. In summary, the Y-shaped branches etched at corners play an important role in improving angular stability and bandwidth.

Given that the direction of incoming wave is unknown, the angular stability is a crucial metric for evaluating the performance of an FSS. Figure 3E,F illustrate the simulated transmission coefficients for both TE and TM polarizations at various incident angles. Excellent angular stability of the FSS is observed. The results reveal a bandwidth of 16.4 GHz for both TE (19.3–37.0 GHz) and TM (20.4–36.8 GHz) polarizations with angular stability up to 40° when IL is greater than 20 dB. Moreover, the angular stability can reach 60° while retaining a stopband width of 21.5 GHz (18.7–40.2 GHz) with IL greater than 14 dB.

3 | EQUIVALENT CIRCUIT ANALYSIS

Figure 4A illustrates the equivalent circuit modeling scheme under TM polarization for the proposed FSS. The ITO strips aligned with the incident wave polarization direction generate equivalent inductance L_1, L_2, and L_3. The adjacent patches generate equivalent capacitance C_1 through coupling, while capacitance C_2 results from the gaps between the Y-shaped branches. The equivalent circuit model (ECM) is subsequently built and consolidated in a concise form as shown in Figure 4B, where the inductance L is equivalent to the series connection of L_1, L_2, and L_3, and the capacitance

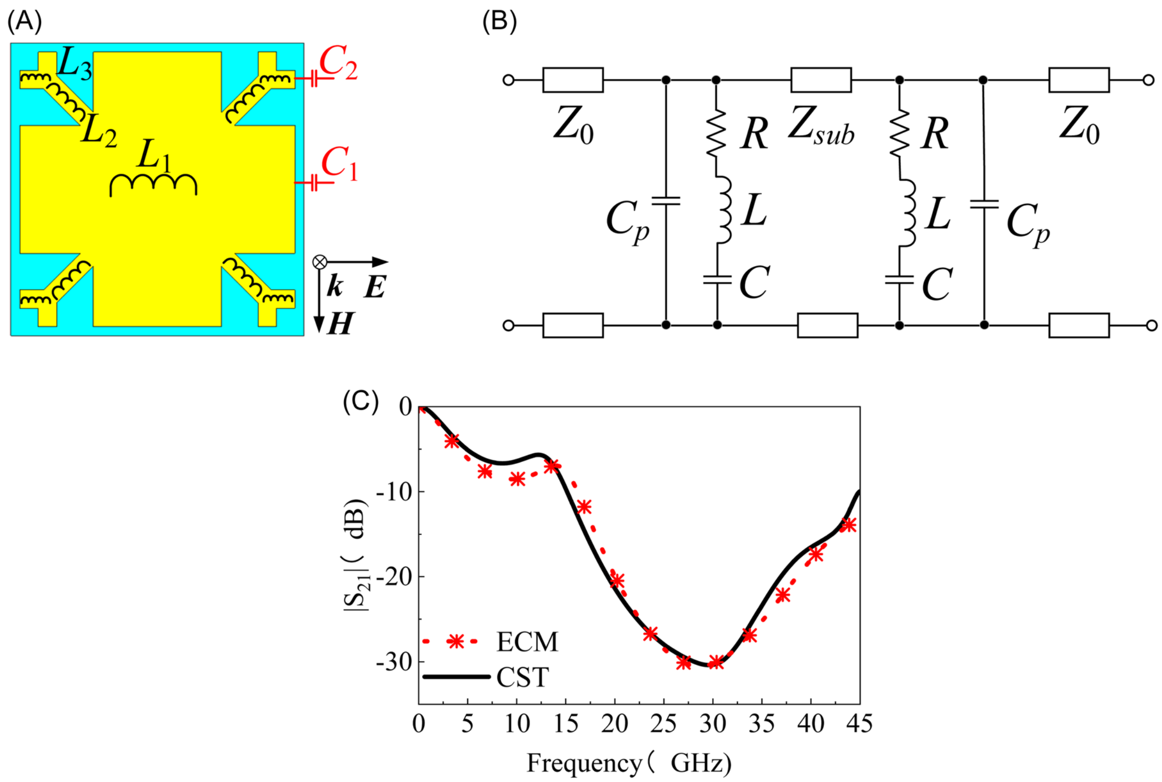

FIGURE 4 (A) Equivalent scheme and (B) simplified equivalent circuit model (ECM) of the frequency selective surface (FSS), where $Z_0 = 377\ \Omega$, $Z_{sub} = 156.5\ \Omega$, $R = 39.5\ \Omega$, $L = 351.5$ pH, $C = 82.0$ fF, and $C_p = 45.0$ fF respectively. (C) $|S_{21}|$ obtained using computer simulation technology and ECM.

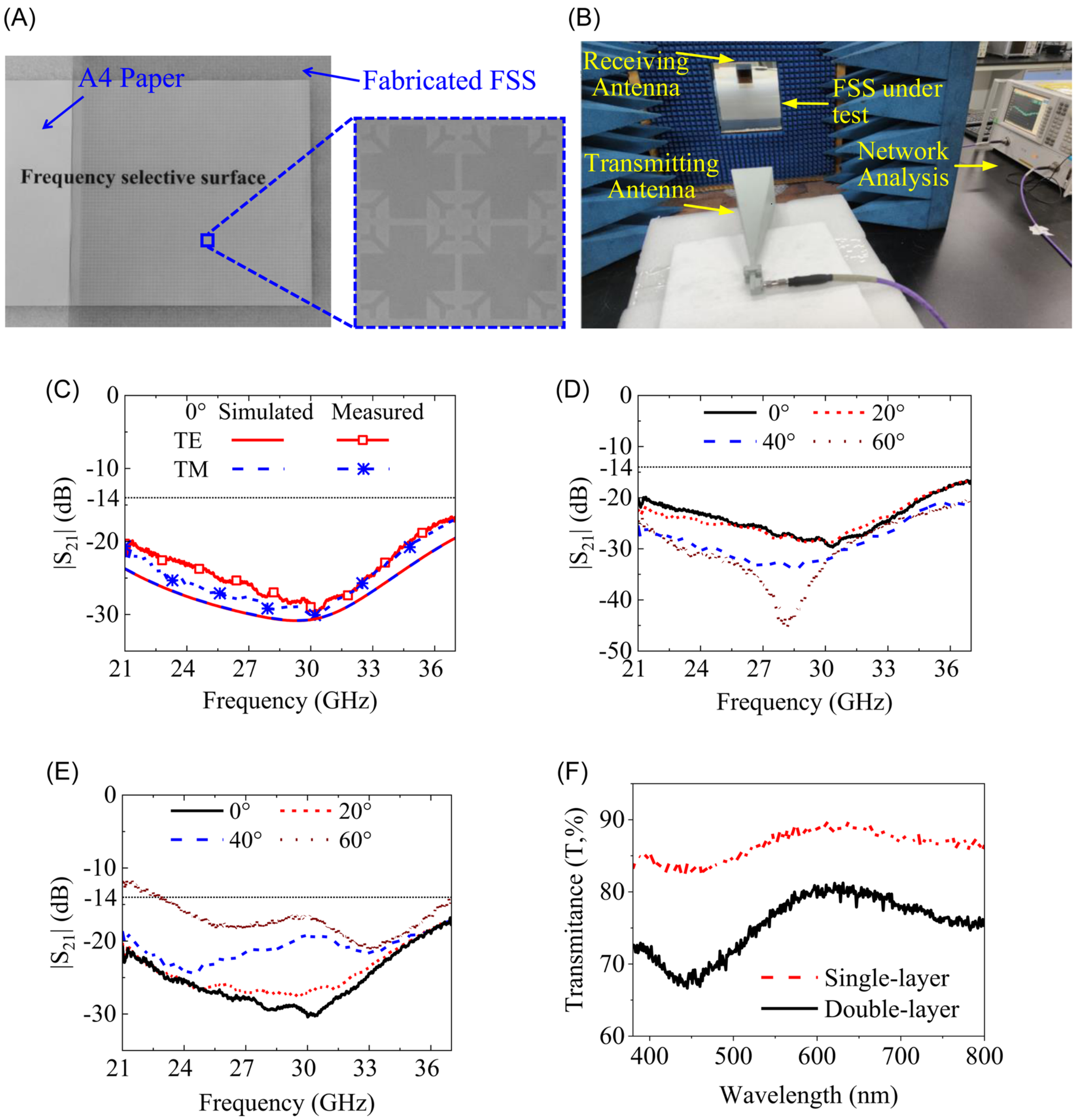

FIGURE 5 (A) Prototype of the proposed transparent frequency selective surface (FSS), and (B) measurement set up. (C) Measured and simulated $|S_{21}|$ under normal incidence. Measured $|S_{21}|$ for (D) TE and (E) TM polarizations. (F) Measured optical transmittance of the prototype.

C is equivalent to the parallel connection of C_1 and C_2, respectively. The finite conductivity of the ITO material contributes to the resistance R in the circuit.[26] A compensating capacitor C_p is connected in parallel with the RLC circuit for precise fitting due to the impedance dispersion.[27,28] The capacitance and inductance values of each segmented strip are approximated from the equations provided in Ref. [29]. After estimating the values of L_1, L_2, L_3, C_1, and C_2, the equivalent L and C in the ECM are then derived. The free space on either side of the FSS is modeled as a transmission line with a characteristic impedance of $Z_0 = 377\,\Omega$. The glass dielectric substrate is equivalent to a short transmission line with a length equal to the substrate thickness in the ECM. Its characteristic impedance is $Z_{sub} = Z_0/\sqrt{\varepsilon_r}$, where the relative dielectric constant of the glass substrate, ε_r, is 5.8. With the aid of the advanced design dystem (ADS),[30] the optimized circuit parameters are obtained and shown in Figure 4. The RLC series circuit generates a stopband at the resonant frequency $f_0 = 1/2\pi\sqrt{LC}$, that is 29.64 GHz. The transmission coefficient obtained from the ECM agrees well with the one simulated using computer simulation technology, as presented in Figure 4C.

TABLE 1 Comparison with the previous works.

References	IL at operation frequency	BW (GHz)/FBW (%) of IL ≥ 14 dB	Transparency (%)	Angular stability (°)
[12]	62.5 dB@3.7 GHz	1.15/28.7	52.5	NM
[13]	43 dB@2.45 GHz and 40 dB@5.5 GHz	0.41/16.5, 1.04/18.8	86	45
[14]	22.7 dB@27.1 GHz	6.9/26.0	44.7	60
[15]	34 dB@29.88 GHz	5.3/17.4	70	NM
[16]	15 dB@0.92 GHz and 12 dB@1.9 GHz	0.15/15.7	81.6	70
[17]	15 dB@16.1 GHz	1.05/6.6	65	NM
[18]	13.8 dB@11.45 GHz and 14.5 dB@24.89 GHz	0.18/0.7	NM	60
[19]	15.6 dB@25.6 GHz	4.47/17.6	72	NM
[20]	14.6 dB@1.75 GHz	0.71/40.7	83 ± 2	30
This work	30.4 dB@29.61 GHz	26.5/89.7	79.5	60

Abbreviation: NM, not mentioned.

4 | EXPERIMENTAL VERIFICATION AND DISCUSSION

A prototype of the double-layer FSS comprising of 87×87 unit cells with a size of 300×300 mm^2 is fabricated by coating the ITO on a glass substrate. The phrase of "Frequency selective surface" printed on an A4 paper is clearly discernible through the fabricated FSS, indicating its good transparency, as shown in Figure 5A. The proposed FSS design is validated through a free-space measurement. Two identical horn antennas were used in the experimental setup, which is illustrated in Figure 5B. One horn antenna, serving as the transmitter, was connected to an Agilent E8363C vector network analyzer, while the other functioned as the receiver. The FSS was placed in between the horn antennas. The transmission coefficient was firstly measured without the FSS in the center. The FSS was then introduced and the transmission coefficient value was re-measured. Finally, the value measured without the FSS was subtracted from the value measured with the FSS to obtain the transmission coefficient specific to the FSS.

Figure 5C–E depict the measured $|S_{21}|$ for various polarizations and incident angles. The results manifest a strong correlation between the measured and simulated $|S_{21}|$, despite few minor deviations. These deviations are mainly attributed to the finite size of the fabricated prototype, manufacturing tolerances, diffraction, and alignment error.

The optical transparency of the prototype was measured in the wavelength range of 380–800 nm using UV-Vis spectrophotometer. As shown in Figure 5F, the single-layer FSS prototype exhibits a high transmittance of over 82%, while the double-layer FSS demonstrates a transmittance of more than 75% across most of the wavelength range, achieving a specific transmittance of 79.5% at the wavelength of 590 nm.

Table 1 compares the proposed transparent FSS design with other similar transparent band-stop FSSs reported in the literature, where the bandwidth (BW) is obtained at normal incidence and the fractional bandwidth (FBW) is calculated. Note that some of the designs in the table have not shown their response stability to oblique incidence. Most of the designs present narrower bandwidths with IL = 14 dB compared with our work. For designs employing opaque conductive materials, the optical transparency of an FSS is calculated as the ratio of the transparent area to the total area of a unit cell.[12,13] The comparison in Table 1 highlights that our proposed band-stop FSS exhibits exceptional rejection of millimeter wave interference, ultra-wide bandwidth, and good angular stability, while preserving excellent optical transparency.

5 | CONCLUSION

A novel optically transparent and angularly stable FSS to mitigate the millimeter wave electromagnetic interference is proposed, particularly designed for integration into the glass doors and windows of buildings. The use of ITO material not only significantly improves overall optical transparency and structural aesthetics but also introduces absorption, leveraging its conductive property to enhance the FSS performance. Simulation results underscore the excellence of our proposed FSS, showcasing exceptional EMI suppression, broad stop band, good angular stability for oblique incidence up to 60°, and superior polarization independence. These features make it highly versatile and appealing for various applications. An equivalent circuit model of the FSS has also been developed and verified by using the full wave simulation. A prototype of the proposed FSS has been fabricated and measured for physical validation. Good agreement observed between experimental and simulated results proves the promising potential of the design. Looking ahead, future iterations of the FSS could explore replacing the glass substrate with other flexible transparent materials, expanding the adaptability of the proposed FSS across a wider range of applications.

ACKNOWLEDGMENTS

This study was supported by National Natural Science Foundation of China under Grant U22A2015.

DATA AVAILABILITY STATEMENT

The data that support the findings of this study are available from the corresponding author upon reasonable request.

ORCID

Liping Yan http://orcid.org/0000-0002-1374-9665
Richard Xian-Ke Gao http://orcid.org/0000-0002-0243-2523
Changjun Liu http://orcid.org/0000-0003-0079-6793

REFERENCES

1. Munk BA. *Frequency Selective Surfaces: Theory and Design*. Wiley; 2000.
2. Yin W, Zhang H, Zhong T, Min X. A novel compact dualband frequency selective surface for GSM shielding by utilizing a 2.5-Dimensional structure. *IEEE Trans Electromagn Compat*. 2018;60(6):2057-2060.
3. Li H, Cao Q, Wang Y. A novel 2-B multifunctional active frequency selective surface for LTE-2.1 GHz. *IEEE Trans Anten Propag*. 2017;65(6):3084-3092.
4. Katoch K, Jaglan N, Gupta SD. Analysis and design of a simple and compact bandstop frequency selective surface at mobile WiMAX and satellite communication x-band. *J Electromag Waves Appl*. 2021;35(10):1321-1336.
5. Katoch K, Jaglan N, Gupta SD, Sharawi MS. Design of a triple band notched polarization independent compact FSS at UWB frequency range. *Int J RF Microw Comput. Aided Eng*. 2021;31(6):1-14.
6. Wang H, Qu S, Wang J, Yan M, Zheng L. Dual-band miniaturised FSS with stable resonance frequencies of 3.4/4.9 GHz for 5G communication systems applications. *IET Microw Anten Propag*. 2020;14(1):1-6.
7. Yadav S, Jain CP, Sharma MM. Smartphone frequency shielding with penta-bandstop FSS for security and electromagnetic health applications. *IEEE Trans Electromagn Compat*. 2019;61(3):887-892.
8. Lin T-H, Kanno K, Watanabe AO, et al. Broadband and miniaturized antenna-in-package. *IEEE Anten Wirel Propag Lett*. 2020;19(11):1963-1967.
9. Li D, Li T-W, Li E-P, Zhang Y-J. A 2.5-D angularly stable frequency selective surface using via-based structure for 5G EMI shielding. *IEEE Trans Electromagn Compat*. 2018;60(3):768-775.
10. Zhang J, Yan L, Gao RX-K, Wang C, Zhao X. A novel 3D ultra-wide stopband frequency selective surface for 5G electromagnetic shielding. *Proceedings of International Symposium on Electromagnetic Compatibility*. 2020:1-4.
11. Yan L, Xu L, Gao RX-K, Zhang J, Yang X, Zhao X. Angularly independent frequency selective surface with good ventilation for millimeter wave EM shielding. *IEEE Trans Electromagn Compat*. 2022;64(1):251-254.
12. Can S, Kapusuz KY, Yilmaz AE. Optically transparent frequency selective surface for ultrawideband applications. *Microw Opt Technol Lett*. 2017;59(12):3197-3201.
13. Farooq U, Shafique MF, Mughal MJ. Polarization insensitive dual band frequency selective surface for RF shielding through glass windows. *IEEE Trans Electromagn Compat*. 2020;62(1):93-100.
14. King DJ, Hettak K, Chaharmir MR, Gupta S. Flexible Ink-minimized screen-printed frequency selective surfaces with increased optical transparency for 5G electromagnetic interference mitigation. *IEEE Trans Compon Packag Manuf Technol*. 2023;13(1):110-119.
15. Mantash M, Kesavan A, Denidni TA. Highly transparent frequency selective surface based on electrotextiles for on-chip applications. *IEEE Anten Wirel Propag Lett*. 2019;18(11):2351-2354.
16. Yang Y, Li W, Salama KN, Shamim A. Polarization insensitive and transparent frequency selective surface for dual band GSM shielding. *IEEE Trans Anten Propag*. 2021;69(5):2779-2789.
17. Song HJ, Schaffner JH, Son KA, Moon JS. Optically transparent Ku-band silver nanowire frequency selective surface on glass substrate. *IEEE Antennas and Propagation Society International Symposium (APSURSI)*. 2014:2100-2101.
18. Hettak K, Shaker J. Screen-printed dual-band flexible frequency selective surface for 5G applications. *European Microwave Conference (EuMC)*. 2019:519-522.
19. Green RB, Guzman M, Izyumskaya N, et al. Optically transparent antennas and filters: a smart city concept to alleviate infrastructure and network capacity challenges. *IEEE Anten Propag Magaz*. 2019;61(3):37-47.
20. Lu Z, Han Y, Zhang W, Li B. Optical-transparent frequency selective surface with wide stopband using indium tin oxide. *International Conference on Microwave and Millimeter Wave Technology Proceedings*. 2020:1-3.
21. Tang L, Yan L, Zhao X, Li X, Jin Y, Gao RX-K. A transparent ultra-wide stopband frequency selective surface for millimeter wave electromagnetic shielding. *Asia-Pacific Symposium on Electromagnetic Compatibility (APEMC)*. 2022:554-556.

22. Parker EA, Antonopoulos C, Simpson NE. "Microwave band FSS in optically transparent conducting layers: performance of ring element arrays. *Microw Opt Technol Lett*. 1997;16(2): 61-63.
23. Aliyu MM, Hossain S, Husna J, et al. High quality indium tin oxide (ITO) film growth by controlling pressure in RF magnetron sputtering. *IEEE Photovoltaic Specialists Conference*. 2012:002009-002013.
24. Zhao Z, Shi H, Guo J, Li W, Zhang A. Stopband frequency selective surface with ultra-large angle of incidence. *IEEE Anten Wirel Propag Lett*. 2017;16:553-556.
25. Kundu D, Mohan A, Chakrabarty A. Comment on 'wide-angle broadband microwave metamaterial absorber with octave bandwidth. *IET Microw Anten Propag*. 2017;11(3):442-443.
26. Ghosh S, Srivastava KV. A dual-band tunable frequency selective surface with independent wideband tuning. *IEEE Anten Wirel Propag Lett*. 2020;19(10):1808-1812.
27. He F, Si K, Li R, et al. Broadband frequency selective surface absorber with dual-section step-impedance matching for oblique incidence applications. *IEEE Trans Anten Propag*. 2021;69(11):7647-7657.
28. Santos EP, Filgueira JDB, Campos ALPS, Gomes Neto A, Maniçoba RHC. Optimization of frequency selective surfaces with crossed dipoles using the Taguchi's method. *J Microw Optoelectron Electromag Appl*. 2017;16(2):371-384.
29. Sarabandi K, Behdad N. A frequency selective surface with miniaturized elements. *IEEE Trans Anten Propag*. 2007;55(5): 1239-1245.
30. Advanced Design System 2020 Documentation. https://edadocs.software.keysight.com/display/engdocads/ADS+2020

How to cite this article: Tang L, Wang C, Yan L, Gao R-K, Zhao X, Liu C. Optically transparent and angularly stable broad-stopband frequency selective surface for millimeter wave electromagnetic interference mitigation. *Microw Opt Technol Lett*. 2024;66:e34078. doi:10.1002/mop.34078